DETECTION AND MODELING OF VISIBLE ALBEDO DUE TO SURFICIAL ICE AT THE LUNAR SOUTH POLE. J. K. Ando[1,2] and S. Li[1], [1]Hawaii Institute of Geophysics and Planetology, University of Hawaii at Manoa, [2]jkando@hawaii.edu

Introduction: Surface exposed water ice has been directly detected inside permanently shadowed regions (PSRs) at the lunar poles using IR spectroscopy from M^3 [1]. Water ice has strong reflectance in the visible to near infrared region (~0.2–1 μm), and high albedo in the visible image data due to water ice was observed on Mercury and Ceres [2]. However, an albedo increase due to surface exposed water ice (if any) has not been detected in the long-exposure images (centered near 0.7 μm) taken by the Narrow Angle Camera (NAC) on the Lunar Reconnaissance Orbiter (LRO) [3,4].

We use the M^3 water ice detections in conjunction with LROC NAC long-exposure images (20 m/pixel) [4] to assess whether albedo enhancements in NAC data will present at the water ice exposures seen by M^3. Also, to understand the detection limit of water ice based on the albedo enhancement in the visible region (e.g., NAC and ShadowCam data), we use Hapke's radiative transfer model (RTM) [5] to model reflectance of ice-regolith intimate mixtures at different wt%.

Methods & Data: We used the IR detections of water ice in 14 PSRs near the lunar south pole, which range in age and ice content [6]. This dataset includes several craters of interest for future in-situ exploration. We assume that the NAC pixel showing the maximum albedo among 196 pixels that were covered by an ice bearing pixel of M^3 data probably contains the highest ice content. We also derive the maximum albedo of 196 NAC pixels in the neighboring M^3 pixels that do not show ice exposures. We then calculate the percent difference of NAC albedo between the most probable ice-bearing NAC pixel and those ice-free neighboring pixels. In each PSR we perform the same procedure at an equal number of random, iceless locations in the same PSR. We do this 50 times for each PSR, to approximately determine the possible range of shifts due to random, non-ice sources of albedo variation. If M^3 detections exhibit a higher median percent shift than random samples, it could be interpreted as due to the presence of water ice.

Hapke modelling of ice-regolith mixtures. Hapke's RTM describes radiance factor *I/F* as a function of viewing geometry (incidence *i*, emittance *e*, phase angle *g*) , average single scattering albedo (SSA) ω_{ave}, backscatter, and phase function $P(g)$ for an intimate particle mixture. For a mixture, $\omega_{ave} = \sum \frac{M_i \omega_i}{\rho_i d_i} / \sum \frac{M_i}{\rho_i d_i}$ and phase $P_{ave} = \sum \frac{M_i \omega_i P_i}{\rho_i d_i} / \frac{M_i \omega_i}{\rho_i d_i}$, where M_i is mass fraction ($\sum M_i = 1$), ρ_i is density, d_i is average particle diameter, ω_i is SSA, and P_i is phase for each material component i. For regolith, we use the LROC Wide Angle Camera phase function [7], and describe our method for approximating ω_{reg} below. For ice, we use a Martian polar ice phase function [8] and experimentally determined optical constants [9].

We select a PSR imaged by NAC with no IR ice detections. As NAC PSR images have unknown secondary illumination, we approximate their reflectance with a scaling factor a, such that $R_{ave} = a\langle I/F \rangle$, where R_{ave} is average regolith reflectance and $\langle I/F \rangle$ is the average unitless "*I/F*" (not true *I/F*, as the *F* used is the solar spectrum, which does not apply to PSR illumination) for the PSR. As the reflectance PSR regolith is unknown, we test two approximate cases: $R_{ave} = 0.075$ for mature (mare-like) regolith, and $R_{ave} = 0.2$ for immature (highlands-like) regolith at $\lambda = 0.7\ \mu m$. We randomly chose 73 280m regions to model ice in. For ice mass fractions M_{ice} from 0.5-20%,

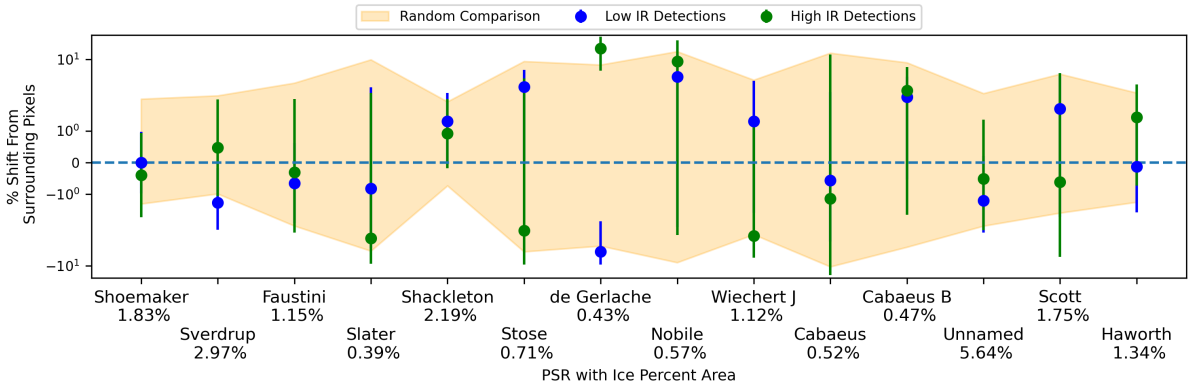

Figure 1: Median percent shift from iceless neighboring pixels for IR detections in fourteen PSRs. Error bars on detections represent 2σ uncertainty on the median. Percentages below PSR names represent the percent of PSRs' area containing ice, based on areas of M^3 IR detections and PSR areas determined from NAC South Pole Mosaic's associated shapefiles [4]. The orange shaded region is the range of equivalent random results for each PSR.

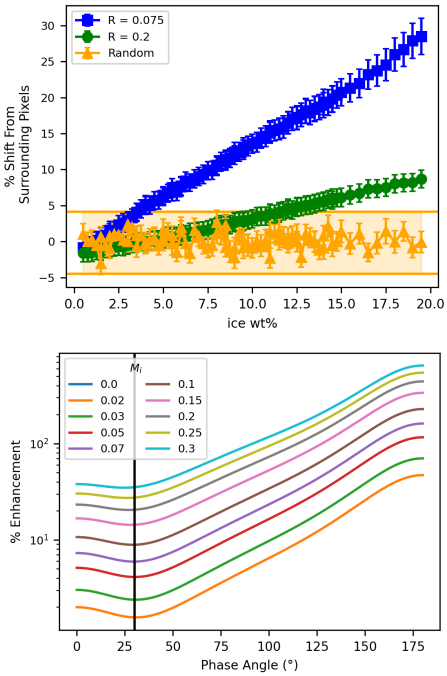

Figure 2: (a) Albedo shift for modeled ice in a PSR, as a function of ice mass fraction. The orange shaded region represents the range of all random samples, which are not affected by M_{ice}. (b) Percent enhancement as a function of phase angle, for different mass fractions of ice, and assuming immature regolith. The black vertical line marks 30°, the viewing geometry used in modeling Fig 2a.

we randomly sampled from a normal distribution with $\mu = M_{ice}$, $\sigma = 0.5\%$.

To model ice, we apply Hapke's RTM to a scaled pixel, assuming standard illumination conditions (i=30°, e=0°, g=30°) to determine ω_{reg}. We then compute the enhanced albedo and phase, with ice at some M_i, and reapply the model to determine the new reflectance. We assume that ice and regolith have an identical average grain size of 70 μm. Once modeled, we apply the same detection procedure as previously described for real M^3 detections.

Results: We examine the median percent shift for each PSR with error on the median alongside random equivalent measurements (Fig 1). We observe no statistically significant shift in any PSR above the range of random data.

Our modelling results demonstrate the efficacy of our method to detect albedo shift. Random samples suggest that a median shift >5% can be interpreted as ice for this PSR (Fig 2a). We determine visible albedo shift due to ice to be detectable if ice abundances are greater than ~15 wt% if regolith is of higher reflectance, and detectable greater than ~5 wt% for low reflectance. Additionally, modeling suggests that the shift is highly dependent on phase (Fig 2b).

Discussion and Future Work: Given the lack of significant albedo enhancements in NAC images indicating the presence of water ice, our modelled thresholds serve as rough upper bounds, meaning ice < ~15 wt%, if our assumptions are valid. This is lower than, but consistent with bounds from M^3 and radar modelling, which both predict up to 30 wt% [1].Both albedo cases are consistent with LAMP UV measurements, which estimate ~0.1-2 wt% ice, if intimately mixed with regolith [10]. Direct detection of ice in Cabaeus crater measured 5.6 ± 2.9 wt% ice [11]—also consistent with immature regolith in our model.

While PSR regolith is not well understood, we believe the immature case is probable. A decrease in nanophase and microphase iron occurs at higher latitudes, inferred as a result of reduced solar wind and micrometeoroid flux, respectively has been observed [12]. South polar PSRs may also be shielded from solar wind by magnetic anomalies [13], further inhibiting nanophase iron formation. Consequently, PSRs may have immature regolith, making visible albedo detections more difficult.

We also find that phase has a major effect on the observed shift. Above ~50° the magnitude of the shift increases roughly exponentially with phase (Fig 2b). Assuming immature regolith, ice as low as 2 wt% could potentially be detectable if observed at $g > 100°$.

Our model represents a rough worst-case scenario, as we choose phase angles, regolith reflectance, and particle size such that enhancement would be roughly at a minimum. Constraining these quantities through viewing geometry modeling of NAC observations can refine these estimates. Laboratory reflectance measurements mimicking PSR secondary illumination may also be viable in constraining the model.

Higher quality datasets, such as those from ShadowCam, may help. However, due to the primary difficulty of detecting ice albedo enhancement being distinguishing it from other dominating sources of albedo variation, ShadowCam's higher sensitivity and spatial resolution may not enable ice detection on its own. We anticipate that high phase angle observations will have the highest probability of detecting ice. We will also reattempt this analysis, instead comparing M^3 to Shadowcam data, as well as modeling the impact of higher resolution data on these methods.

References: [1] S. Li, et al., Proc. Natl. Acad.Sci.115 (2018) 8907–8912. [2] N. Schörghofer, et al., Spac Sci. Rev. 217 (2021) 74. [3] J. Mitchell, et al., Planet.Space Sci. 162 (2018) 133–147. [4] H.M. Brown, et al., Lunar Pol. Vol. Conf. (2022), Abstract # 5033.[5]B. Hapke, J. Geophys. Res. Solid Earth 86 (1981) 3039–3054. [6] A.N. Deutsch, et al., Icarus 336 (2020) 113455. [7] B. Hapke, et al., J. Geophys. Res. Planets 117 (2012). [8] A.C. Pascuzzo, et al., Icarus 374 (2022) 114804. [9] S.G. Warren, R.E. Brandt, J. Geophys. Res. Atmo.113 (2008). [10] P.O. Hayne, et al., Icarus 255 (2015) 58–69.[11] A. Colaprete, et al., Science 330 (2010) 463–468. [12] D. Trang, P.G. Lucey, Icarus 321 (2019) 307–323. [13] L.L. Hood, et al., Geophys. Res. Lett. (2022)